High Temperature Unimolecular Decomposition of Cyclopentanone

Binod Raj Giri[1], Mohammed AlAbbad[1], John R. Barker[2,*] and Aamir Farooq[1,*]

[1]King Abdullah University of Science and Technology (KAUST), Clean Combustion Research Center, Physical Sciences and Engineering Division, Thuwal, Saudi Arabia
[2]Department of Climate and Space Sciences & Engineering, University of Michigan, Ann Arbor, Michigan 48109-2143, United States

*Corresponding Authors: Aamir.Farooq@kaust.edu.sa; jrbarker@umich.edu

Colloquium: Gas-Phase Reaction Kinetics

Word Count (method1):

Main text	3581
Equations: 5	76
References: 33	611.8
Figures: 4	823.2
Tables: 0	0
Total	**5092**

This paper includes Supplementary Material.

Abstract

This work reports thermal decomposition of cyclopentanone behind reflected shock waves over 1150 – 1590 K and 750 – 1800 Torr. Carbon monoxide is one of the main reaction products and its formation was monitored using a quantum cascade laser operating near 4.56 μm. Our results show that cyclopentanone undergoes decomposition, under the present experimental conditions, *via* reaction channels that produce CO almost exclusively. A recent *ab initio* study by Zaras et al. (Int J Chem Kinet 47, 2015, 439-446) revealed that cyclopentanone decomposes to produce CO and ethylene by two channels: ring-opening to form a di-radical which subsequently decomposes, and concerted elimination to produce CO and C_2H_4 directly; their predicted rate constants are much slower than literature experimental data. To resolve the rate constant discrepancy and to determine whether keto-enol tautomerism plays a significant role, we performed master equation simulations which produced results in good agreement both with the previous *ab initio* study and with the experimental data obtained in the present work.

Keywords: *Cyclopentanone; Unimolecular decomposition; Ab initio; Carbon monoxide; Laser absorption.*

1. Introduction

Ketones are of significant interest as potential biofuels. Several researchers have demonstrated the use of chemical and biochemical conversion process technology for biofuel production [1]. One such technology involves using endophytic fungi to decompose lignocellulosic biomass, agro-industrial residues, and wastewater to produce a wide array of volatile organic compounds (VOCs), including saturated and unsaturated hydrocarbons, ketones, esters, acids, and alcohols [1-4]. These oxygenated compounds can promote cleaner combustion by reducing emissions of greenhouse gases and particulates. Ketones are also important intermediates in the low-temperature oxidation of large hydrocarbons and oxygenated fuels such as alcohols and esters. Therefore, the reaction kinetics of ketones is of substantial interest.

Cyclopentanone (CPO) is a five-member ring cyclic ketone that can be efficiently produced from hydrogenation of biomass derived furfural [5], and the pyrolysis of biomass [6] and of nylon 66 [7]. It is highly resistant to auto-ignition and can potentially be utilized in fuel blends for spark-ignition internal combustion engines. It may also prove to be a promising feedstock for synthesis of polycyclic alkanes [8,9] which are known as high-density fuels [10], and it may be used as aviation fuel as well as in blends with increased volumetric heating values. Despite its importance in combustion, the kinetics of CPO has received very little attention [11-17].

Cyclopentanone decomposition has been studied experimentally by using photochemical [11,12] and thermal [13,14] methods, and computationally by *ab initio*/master equation methods [15]. The first study dates back to 1935, when Saltmarsh and Norrish[11] carried out photochemical decomposition of cyclic ketones with *n*-membered rings that contained 5 to 7 carbon atoms ($5 \leq n \leq 7$). They concluded that these cyclic ketones primarily decompose *via* simultaneous rupture of both C-C bonds adjacent to the carbonyl group, forming CO and cyclic alkanes (*n*-1) as final products. However, in the case of CPO, they identified ethylene, butene isomers (C_4H_8) and CO as the decomposition products. They hypothesized that the decomposition of cyclic ketones can produce cyclic hydrocarbons when there is

a possibility for the formation of a 5 or 6 membered ring. In a later photolysis study, Benson and Kistiakowsky [12] suggested that the C_4H_8 identified by Saltmarsh and Norrish [11] as butene isomers is actually cyclobutane (C_4H_8). They questioned the experimental techniques employed by Saltmarsh and Norrish [11] and further stated that the photolysis of cyclic ketones is much more complex than the simple hypothesis advanced by Saltmarsh and Norrish [11]. Somewhat later, Johnson and Walters [13] studied the thermal decomposition of CPO in a cylindrical pyrex reaction vessel at 761 – 816 K and 99 – 314 Torr, and reported that the major products in the early stages of reaction are CO, C_2H_4, H_2, 1-butene, 2-cyclopenten-1-one. They found that the reaction is not elementary since it exhibited an induction period and was autocatalytic, i.e., it was accelerated by the addition of the reaction products. In the most recent experimental study of CPO, Delles et al. [14] conducted experiments at 805 – 854 K and 11 – 30 Torr, and observed major products similar to those reported by Johnson and Walters [13] but they additionally identified 4-pentenal as an important product, and reported that the over-all thermal decomposition of CPO can be described by $k(T) = 1.5 \times 10^{12} \exp(-29642.7/T)$ s^{-1}. Delles et al. [14] confirmed that the reaction is autocatalytic and also that its rate is reduced by the addition of nitric oxide, suggesting participation by a free radical chain mechanism under their conditions. All of these experimental studies were confined to temperatures lower than 855 K and the most recent study [14] was performed almost 50 years ago.

Recently, Zaras et al. [15] employed G3B3/master equation-RRKM computational methods to investigate the various decomposition pathways for CPO decomposition. The authors [15] were able to map out seven different reaction routes that led to the major decomposition products observed previously in the pyrolysis experiments. Their calculations showed that the reaction route leading directly to C_2H_4 and CO is the dominant channel and is significantly faster than keto-enol tautomerism, particularly at high temperatures. The authors further reported that enolization is less favored in CPO than in cyclohexanone, since the latter has a lower barrier for the corresponding reaction. Their calculated rate coefficients for CPO decomposition are at least an order of magnitude slower than the

experimental rate expression reported by Delles et al. [14].

The present work was motivated by the discrepancy between theory and experiment and by the problems encountered in the early experimental works which employed classical macroscopic kinetics techniques. Experimental techniques have advanced greatly since those days. The objectives behind the present work are several-fold: (i) obtain experimental rate constants for the thermal decomposition of CPO at high temperatures which are more relevant for combustion systems, (ii) perform statistical rate theory calculations for comparison to the experiments and attempt to resolve the discrepancy between theory and experiment, (iii) assess of the role of the keto-enol tautomerization channel.

2. Experimental Setup

Thermal unimolecular decomposition of cyclopentanone (CPO) was investigated in the low-pressure shock tube (LPST) facility at King Abdullah University of Science and Technology (KAUST). As the details of LPST can be found elsewhere [18], we provide here only a brief description. The LPST, fabricated from stainless steel, has driver and driven sections with an inner diameter of 14.2 cm. The length of the driver section can be varied to achieve the desired reaction time behind reflected shock waves. This work used a 3 meter long driver section to achieve test times of about 1.5 ms. The driven section was separated from the driver section by a polycarbonate diaphragm. To ensure high purity prior to each experiment, the driven section was pumped down to $<10^{-5}$ Torr using a turbo-molecular pump and the driver section was evacuated to 10^{-3} Torr. Thereafter, the driven and driver sections were filled with the cyclopentanone-argon mixture and helium gas, respectively. Shock waves were generated by gradually increasing the helium pressure in the driver section until the diaphragm ruptured. The incident shock wave speed was measured by a series of five PCB 113B26 piezoelectric pressure transducers (PZTs) placed in the last 1.3 m of the driven section. All experiments were conducted behind reflected shock waves, and the post-shock conditions (T_5, P_5) were calculated, with

a maximum uncertainty of 1%, using standard shock-jump relations [19] embedded in the Frosh code. [20]. Optical windows for the CO laser diagnostic and a Kistler PZT were located at 2 cm from the shock tube endwall.

Carbon monoxide was monitored using the R(13) absorption line near 2193.36 cm^{-1} (4.56 μm) in the ν_1 fundamental vibrational band of CO. A fixed-wavelength direct absorption strategy was used, where the mid-IR light was generated by a cw quantum cascade laser (QCL) supplied by Alpes Lasers. The mole fraction of CO was obtained using the Beer-Lambert law: $I/I_0 = \exp(-S\phi x_i P_5 L)$ where I and I_0 are the transmitted and incident laser intensities, respectively; S (cm^{-2} atm^{-1}) is the line-strength of the ro-vibrational absorption transition, ϕ(cm) is the line-shape function, x_i is the mole fraction of the absorbing species, P_5 (atm) is the total pressure of the gas behind the reflected shock wave and L (cm) is the absorption path length (internal diameter of the shock tube). Argon-broadening parameters for the R(13) transition were taken from Ren et al.[21] and the line-strength was obtained from the HITRAN database [22].

Gas mixtures of cyclopentanone (≥99% Sigma-Aldrich; further purified through freeze-pump-thaw cycles), diluted in argon (99.999%) were prepared manometrically in a 24 L teflon-coated stainless steel vessel equipped with a magnetically driven stirrer. Prior to mixture preparation, the vessel was pumped down to $<10^{-5}$ Torr. Mixtures were allowed to homogenize for at least two hours before use, and contained 0.2 – 1.2% CPO in argon.

3. Results and Discussion

3.1 Cyclopentanone Decomposition Pathways

The major reaction pathways for the unimolecular decomposition of cyclopentanone are shown in Fig. 1. The energetics for these pathways are taken from Zaras et al. [15] who used the G3B3 method to compute the stationary points on the potential energy surface (PES).

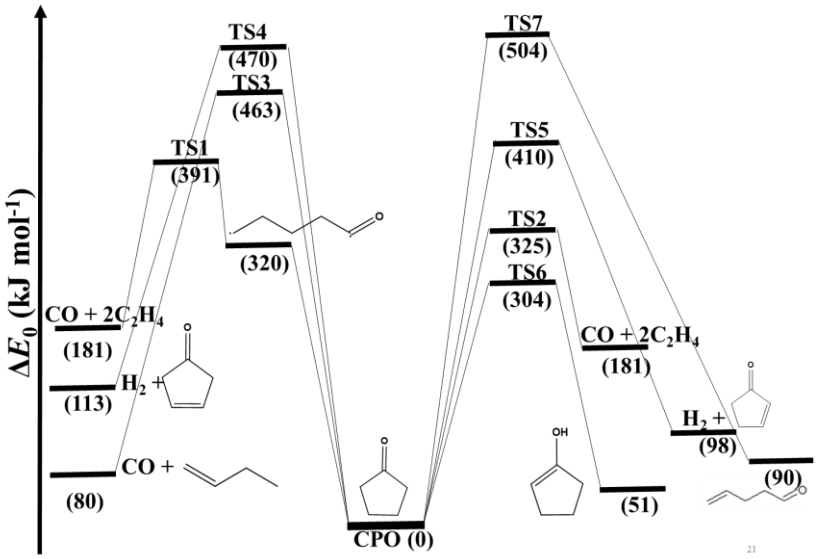

Fig. 1. G3B3 energies [15] for the major decomposition pathways of cyclopentanone (CPO).

As shown in Fig. 1, the energy barriers for the reaction pathways *via* TS3, TS4, TS5, and TS7 are significantly higher than those proceeding *via* TS1, TS2 and TS6. Zaras et al. [15] predicted that the higher energy channels make negligible contributions to the total decomposition rate. This suggests that the higher energy channels can safely be neglected in the analysis of our kinetic data, leaving only the following three reactions to be considered:

CPO → $^{\bullet}CH_2(CH_2)_3C^{\bullet}=O$ (R1a)

CPO → CO + 2 C_2H_4 (R2)

CPO → cyclopentenol → → various products (R3)

Two distinct reaction pathways, R1 and R2, which occur via TS1 and TS2, respectively, lead to the same set of products: CO and C_2H_4. Reaction pathway R1, which is indirect, first surmounts a thermodynamic barrier of 326.8 kJ/mol (reaction R1a has no intrinsic barrier) to open the ring and produce an open chain diradical ($^{\bullet}CH_2(CH_2)_3C^{\bullet}=O$), which reacts further by a low energy path (reaction R1b with an energy barrier of 64.4 kJ/mol relative to the diradical) to produce CO and C_2H_4. As shown in Fig. 4 of Zaras et al. [15], the open chain diradical can also isomerize to 4-pentenal by overcoming an energy barrier of 301.3 kJ/mol (reaction R1c – not shown in Fig. 1). However, reaction R1c is not important, because its barrier height is so much greater than that of reaction R1b.

$^{\bullet}CH_2(CH_2)_3C^{\bullet}=O \rightarrow CO + 2\ C_2H_4$ (R1b)

$^{\bullet}CH_2(CH_2)_3C^{\bullet}=O \rightarrow CH_2=CHCH_2CH_2C(H)=O$ (R1c)

Reaction R2, the second pathway that produces CO and C_2H_4, proceeds directly in a concerted manner via TS2.

A third pathway, reaction R3, proceeds first by an enolization step to produce cyclopentenol (keto-enol tautomerization via TS6 with energy barrier 304 kJ/mol), which reacts further to produce various products, as shown in Figure 4 of Zaras et al. [15]. The enolization step via TS6 has a higher energy barrier than the analogous process in cyclohexanone (276 kJ/mol [23]), but it is lower in energy than pathways R1 and R2. Although it is lower in energy, the CPO enolization reaction on pathway R3 has a very tight transition state ($\Delta S_{298.15K}^{\neq}$ = -3.3 J mol^{-1} K^{-1}), while the transition states along pathways R1a and R2 are much looser ($\Delta S_{298.15K}^{\neq}$ = 18 -38.5 and 40.2 J mol^{-1} K^{-1}, respectively). The net result is that the channels producing CO and C_2H_4 are more important than channel R3.

For the analysis of experimental data, a further simplification is possible (and supported by the theoretical calculations described below). Because reactions R1b and R1c occur via tight transition states with significant energy barriers, while the reverse of reaction R1a (recyclization of the open

chain diradical) is barrierless and hence very rapid, subsequent reaction to form CO + C_2H_4 cannot compete with R2. Therefore, the indirect channel forming CO and C_2H_4 can be neglected in analyzing the experimental data on CPO decomposition.

3.2 Experimental Rate Coefficients

From the discussion above, the most favored decomposition channels of CPO decomposition are expected to be the reactions R2 and R3. R2 forms CO and C_2H_4 directly, while R3 is the enolization channel which eventually leads to the formation of other products. Because CO is one of the major products, we monitored the evolution of CO to extract the kinetic information. Our results show that the CO yield approaches unity ($[CO]_\infty/[CPO]_0 \approx 1$) at high temperatures and/or long reaction times (see Fig. 2). Moreover, the measured evolution of CO starts at the onset of reaction at high temperatures which clearly indicates that R2 is the major decomposition pathway. This observation is consistent with the theoretical predictions of Zaras et al. [15].

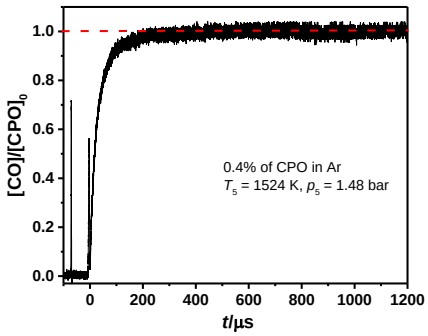

Fig. 2. Measured $[CO]/[CPO]_0$ time history for the thermal unimolecular decomposition of cyclopentanone (CPO). The red line shows that CO yield reaches unity at high temperatures and/or long reaction times.

The reaction rate coefficients $k(T, p)$ were extracted by iteratively varying the rate coefficients for R2 and R3 until the best fit of the measured absorbance time-profiles of CO was obtained. ChemkinPro was used for the kinetic simulation using the detailed cyclopentanone oxidation mechanism from Thion et al. [16], and the initial estimates of the rate coefficients for R2 and R3 were taken from Zaras

et al. [15]. The best-fit kinetic simulations are shown in Fig. 3 and the total rate coefficients for the loss of CPO in each experiment are plotted in Fig. 4 (and compiled in Table S1 of the Supporting Information). The measured rate coefficients, obtained at pressures ranging from 750 to 1800 Torr, did not exhibit any discernible pressure dependence. This suggests that the CPO decomposition is close to the high-pressure limit under the present experimental conditions.

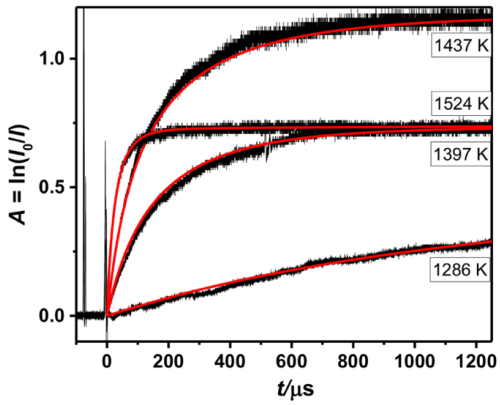

Fig. 3. Representative absorbance time-profiles for the formation of CO from the thermal decomposition of cyclopentanone. Black lines are the experimental traces and red lines indicate the best fit of kinetic simulations at the specified temperatures. Further details of the experimental conditions are provided in Table S1 of the Supporting Information.

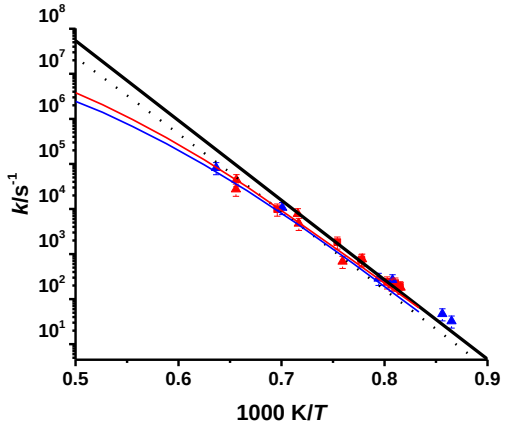

Fig. 4. Arrhenius plot for the experimental and theoretical rate coefficients for the thermal decomposition of cyclopentanone. Symbols: experimental data from this work; (▲) 735 – 975 Torr, (▲) 1050 – 1350 Torr, (■) 1425 – 1800 Torr. Solid lines: results of our master equation calculations for $p = \infty$, 1500 and 750 Torr; (….) Zaras et al. [15] values for the total high-pressure limiting rate coefficients. The error bars (±25%) of our measured rate constants account uncertainties in the temperature (±1%) of reflected shock wave, location of time zero (±0.5 μs), mixture composition (±5%), CO absorption cross section (~3%).

Our experimental data compare reasonably well with the theoretical predictions of Zaras et al. [15] (dashed line in Fig. 4), except for the difference in temperature-dependence and, at the lower temperatures, the experimental rate constants are at least twice as fast as the k_∞ predicted by Zaras et al. [15]. This suggests that the energy barriers predicted by the theory for the low-lying channels are somewhat too high. For that reason, we empirically reduced the energy barrier of TS2 (direct pathway to $CO+C_2H_4$) by 6.3 kJ/mol (1.5 kcal/mol), which is within the range of accuracy expected for this level of theory. After making this adjustment, the computed pressure- and temperature- dependent rate coefficients (solid lines in Fig. 4) and branching ratios are in good agreement with the experimental data as described in the next section.

3.3 Master Equation Simulations

Pressure- and temperature- dependent rate coefficients were computed by using the MultiWell Master Equation Program Suite [24-26]. MultiWell uses stochastic simulations to solve the 1-D master equation which depends on total internal energy, as outlined by Smith and Gilbert [27] and slightly extended by others [28]. Full descriptions of the code and underlying theory can be found in the literature citations and the User Manual.

In these calculations, argon was used as bath gas and the energy transfer was treated using the exponential-down model with $\langle\Delta E\rangle_d = 200\ (T/300K)^{0.85}$ cm^{-1} [15,23,29]. The bimolecular rate coefficients describing the collisions between argon and the reactant molecule or the intermediate wells are based on Lennard-Jones (LJ) collisions parameters, which were obtained from the parameters of the individual collision partners by using the standard combination rules. The LJ parameters used were σ = 3.47 Å and ε/k_b = 114 K for Ar [30], and σ = 5.5 Å and ε/k_b = 650.7 K for CPO [15]. For the molecular properties, we used the G3B3 parameters reported by Zaras et al. [15] for reactions R1, R2 and R3 except for the missing parameters for the step cyclopentenol → cyclopentadienol + H_2 of the reaction sequence R3. For this step, we performed additional G3B3 calculations (with the same basis

set used by Zaras et al. [15]) to obtain the energetics and transition state molecular parameters. The calculated value of the barrier height for this step is found to be 251 kJ/mol, in exact agreement with Zaras et al. [15]. The molecular parameters and the geometries are listed in Table S2 and S3 of the Supporting Information.

Most of the rate constants in the master equation calculations were calculated from the molecular parameters by using the RRKM theory, i.e., microcanonical transition state theory (TST). Angular momentum-resolved microcanonical variational TST (i.e., VTST) theory was used to compute rate constants for the barrierless reaction R1a. For that purpose, the molecular parameters were taken from Zaras et al. [15], who performed relaxed scans at fixed points along the reaction path between 2.1 and 3.5 Å at intervals of 0.1 Å (defined by the fissioning C–C bond distance). These parameters were used by the code MultiWell/Ktools to compute the microcanonical VTST rate constants for reaction path R1a (the Ktools input data are reported in Supporting Information). The rotational and vibrational parameters of the transition state for reaction R1b were not reported by Zaras et al. [15]. Since this reaction is expected to be a minor pathway, the microcanonical rate constants needed for the calculations were computed using the Inverse Laplace Transform (ILT) method [31], based on the critical energy reported by Zaras et al. [15] and an assumed Arrhenius *A*-factor, $A_\infty = 10^{14}$ s^{-1}, which is appropriate for a tight transition state at the temperatures of interest [32]. Tests performed by using the methods outlined below showed that the calculated values for k_{uni} increased by only ~10% when this *A*-factor was increased by a factor of 100.

At each temperature and pressure, master equation simulations were performed for simulated time periods corresponding to 10^4 collisions (the MultiWell input data are reported in Supporting Information). In each case, the number of stochastic trials was set to 10^5 or 10^6, in order to reduce stochastic noise to the level of ≤ 3% (1 standard deviation). After the initial transient period (≤ 500 collisions in this case, based on stabilization of the average vibrational energy [33]) the simulated decays of CPO were very nearly pure exponential functions and unimolecular rate constants were

evaluated by assuming a pure exponential decay: $k_{uni} = \ln(f_2/f_1)/(t_2-t_1)$, where f_i is the fraction of CPO at time t_i; t_1 and t_2 corresponded to 10^3 and 10^4 collisions, respectively.

The results of our calculations are summarized in Fig. 4 and in Tables S4 – S6 (Supporting Information) which report values of k_{uni}, the stochastic uncertainties, and branching ratios for the various pathways, respectively. As can be seen in Fig. 4, our calculated values of the high-pressure limiting rate coefficients, $k_\infty(T)$, agree well with the experimental data, thus supporting the conclusion that our experimental data are close to the high-pressure limit, perhaps somewhat below it. Most of our experiments were carried out at pressures ranging from 1 to 2 bar, where pressure falloff makes a contribution. The pressure falloff observed in the experiments at higher temperatures is captured well by our master equation calculations, as shown in Fig. 4. Our calculations also predict that the decomposition of CPO leads almost exclusively to CO and C_2H_4 ($\geq$ 95%) via reaction R2 under our experimental conditions, and that the reaction R1 is negligible. The lowest energy pathway (R3) contributes $\lesssim$ 3% to the total product yield.

The calculations described above were performed after making a single empirical adjustment to the *ab initio* quantum chemistry results i.e lowering the energy of TS2 by 6.3 kJ/mol (1.5 kcal/mol) below the G3B3 value. We performed additional tests (at 1500 K and 1.5 bar) to determine whether adjusting the energy of TS6 (without adjustments to any of the other *ab initio* energies) could achieve similar good agreement with the experimental data. We found that when the energy of TS6 is lowered by 30 kJ/mol (a much greater adjustment than the expected errors in the quantum chemistry calculations), the predicted rate constant is still >15% too low, and the branching ratio for reaction R2 is only 71%, which is much smaller than the experimental value. It might be possible to match the experimental value for the unimolecular rate constant by making larger adjustments to the barrier height of TS6, but then the predicted branching ratio would be even smaller. We conclude that the semi-empirical model utilizing the adjusted barrier for TS2 provides the best description of the reaction system that is

currently available.

The calculated sum of the high-pressure limiting rate coefficients for all channels can be expressed as $k_\infty(T) = 3.2 \times 10^{16} \exp(-336 \text{ kJ mol}^{-1}/RT) \text{ s}^{-1}$ for temperatures in the range 800 – 2000 K. This total high-pressure rate constant and the extrapolated values of the experimental rate constants measured in the present work are lower than the results reported by Delles et al. [14], despite the fact that their experiments were performed at much lower pressures and, therefore, pressure fall-off should have been more important. Their results (and those of Johnson and Walters [13]) showed clear evidence of an induction period, autocatalysis, and quenching by nitric oxide, which suggested to them that the reaction was proceeding at least in part by a free radical chain. The present results are consistent with their interpretation and we conclude that the present results are a more accurate description of the unimolecular reactions of cyclopentanone.

4. Conclusions

The kinetics of the thermal decomposition of cyclopentanone was studied behind reflected shock waves at 1150 – 1590 K and 750 – 1800 Torr. Our measured rate coefficients did not show a significant pressure effect which shows that the measured data are close to the high-pressure limit. Our measured CO yield was found to be ~ unity at high temperatures, suggesting that the reaction R2 is the major channel. We found that reaction R1, which also eventually produces CO and C_2H_4, contributes negligibly small to the CO yield. Our master equation results are consistent with the experimental rate constants and product yields reported in the present work. These predict that reaction R2 contributes ≥ 95% to cyclopentanone decomposition under our experimental conditions, whereas reaction R3 contributes ≲ 3%. Our experimental results are superior to previous experiments which were probably

affected by secondary free radical chain reactions. In addition, master equation calculations and consequent simulation and modeling underpin an enhanced understanding of the underlying chemistry.

Acknowledgments

Research reported in this work was funded by King Abdullah University of Science and Technology (KAUST). JRB thanks the University of Michigan for partial support of this work.

List of Figures (in the Manuscript):

Fig. 1. G3B3 energies [15] for the major decomposition pathways of cyclopentanone (CPO).

Fig. 2. Measured $[CO]/[CPO]_0$ time history for the thermal unimolecular decomposition of cyclopentanone (CPO). The red line shows that CO yield reaches unity at high temperatures and/or long reaction times.

Fig. 3. Representative absorbance time-profiles for the formation of CO from the thermal decomposition of cyclopentanone. Black lines are the experimental traces and red lines indicate the best fit of kinetic simulations at the specified temperatures. Further details of the experimental conditions are provided in Table S1 of the Supporting Information.

Fig. 4. Arrhenius plot for the experimental and theoretical rate coefficients for the thermal decomposition of cyclopentanone. Symbols: experimental data from this work; (▲) 735 – 975 Torr,

(▲) 1050 – 1350 Torr, (■)1425 – 1800 Torr. Solid lines: results of our master equation calculations for p = ∞, 1500 and 750 Torr; (….) Zaras et al. [15] values for the total high-pressure limiting rate coefficients. The error bars (±25%) of our measured rate constants account uncertainties in the temperature (±1%) of reflected shock wave, location of time zero (±0.5 μs), mixture composition (±5%), CO absorption cross section (~3%).

List of Supplementary Materials:

Table S1. Measured rate coefficients with the experimental conditions. The uncertainty associated with the rate coefficients is ~ ±25%.

Table S2. Calculated G3B3 unscaled harmonic vibrational wavenumbers and rotational constants for cyclopentenol → cyclopentadienol + H_2 reaction in the potential energy surface of cyclopentanone decomposition – see Zaras et al. [15] for the reaction pathways. For all other primary decomposition pathways of cyclopentanone, the molecular parameters were taken from Zaras et al. [15]. Imaginary wavenumber is denoted by i.

Table S3. Calculated B3LYP/6-31G(d) geometries in Cartesian coordinates of the stationary points for the decomposition pathway cyclopentenol → cyclopentadienol + H_2.

Table S4. Total unimolecular rate constant (k_{uni} / s^{-1}) and statistical errors.

Table S5. Percent yield of CO + 2 C_2H_4.

Table S6. Percent yield of cyclopentenol (C_5H_7OH) from enolization reaction.

Input Data Files for The MULTIWELL Program Suite.

References

[1] R. Luque, C.S.K. Lin, K. Wilson, J. Clark, Handbook of biofuels production Processes and Technologies, Woodhead Publishing, Amsterdam u.a, 2016.

[2] G.A. Strobel, B. Knighton, K. Kluck, Y. Ren, T. Livinghouse, M. Griffin, D. Spakowicz, J. Sears, Microbiology 154 (2008) 3319.

[3] A. Yousuf, F. Sannino, V. Addorisio, D. Pirozzi, J. Agric. Food. Chem. 58 (2010) 8630.

[4] X.-f. Chen, C. Huang, L. Xiong, X.-d. Chen, Y. Chen, L.-l. Ma, Bioresour. Technol. 118 (2012) 594.

[5] M. Hronec, K. Fulajtarová, Catal. Commun. 24 (2012) 100.

[6] A. Demirbas, Fuel Process. Technol. 88 (2007) 591.

[7] A. Ballistreri, D. Garozzo, M. Giuffrida, G. Montaudo, Macromolecules 20 (1987) 2991.

[8] J. Yang, N. Li, G. Li, W. Wang, A. Wang, X. Wang, Y. Cong, T. Zhang, Chem. Commun. 50 (2014) 2572.

[9] W. Wang, N. Li, G. Li, S. Li, W. Wang, A. Wang, Y. Cong, X. Wang, T. Zhang, ACS Sustainable Chemistry & Engineering 5 (2017) 1812.

[10] H.S. Chung, C.S.H. Chen, R.A. Kremer, J.R. Boulton, G.W. Burdette, Energy & Fuels 13 (1999) 641.

[11] O.D. Saltmarsh, R.G.W. Norrish, Journal of the Chemical Society (Resumed) (1935) 455.

[12] S.W. Benson, G.B. Kistiakowsky, Journal of the American Chemical Society 64 (1942) 80.

[13] E.R. Johnson, W.D. Walters, Journal of the American Chemical Society 76 (1954) 6266.

[14] F.M. Delles, L.T. Dodd, L.F. Lowden, F.J. Romano, L.G. Daignault, Journal of the American Chemical Society 91 (1969) 7645.

[15] A.M. Zaras, S. Thion, P. Dagaut, International Journal of Chemical Kinetics 47 (2015) 439.

[16] S. Thion, C. Togbé, G. Dayma, Z. Serinyel, P. Dagaut, Energy & Fuels 31 (2017) 2144.

[17] A.M. Scheer, O. Welz, S.S. Vasu, D.L. Osborn, C.A. Taatjes, Physical Chemistry Chemical Physics 17 (2015) 12124.

[18] J. Badra, F. Khaled, B.R. Giri, A. Farooq, Physical Chemistry Chemical Physics 17 (2015) 2421.

[19] J. Bradley, Methuen, London (1962).

[20] M.F. Campbell, D.R. Haylett, D.F. Davidson, R.K. Hanson, Shock Waves (2015) 1.

[21] W. Ren, A. Farooq, D.F. Davidson, R.K. Hanson, Appl. Phys. B 107 (2012) 849.

[22] L.S. Rothman, I.E. Gordon, Y. Babikov, A. Barbe, D. Chris Benner, P.F. Bernath, M. Birk, L. Bizzocchi, V. Boudon, L.R. Brown, A. Campargue, K. Chance, E.A. Cohen, L.H. Coudert, V.M. Devi, B.J. Drouin, A. Fayt, J.M. Flaud, R.R. Gamache, J.J. Harrison, J.M. Hartmann, C. Hill, J.T. Hodges, D. Jacquemart, A. Jolly, J. Lamouroux, R.J. Le Roy, G. Li, D.A. Long, O.M. Lyulin, C.J. Mackie, S.T. Massie, S. Mikhailenko, H.S.P. Müller, O.V. Naumenko, A.V. Nikitin, J. Orphal, V. Perevalov, A. Perrin, E.R. Polovtseva, C. Richard, M.A.H. Smith, E. Starikova, K. Sung, S. Tashkun, J. Tennyson, G.C. Toon, V.G. Tyuterev, G. Wagner, J. Quant. Spectrosc. Radiat.

Transfer 130 (2013) 4.
[23] A.M. Zaras, P. Dagaut, Z. Serinyel, The Journal of Physical Chemistry A 119 (2015) 7138.
[24] T.L.N. J. R. Barker, J. F. Stanton, C. Aieta, M. Ceotto, F. Gabas, T. J. D. Kumar, C. G. L. Li, L. L. Lohr, A. Maranzana, N. F. Ortiz, J. M. Preses, J. M. Simmie, J. A. Sonk, and P. J. Stimac, MultiWell-2017 Software Suite, 2017.
[25] J.R. Barker, International Journal of Chemical Kinetics 33 (2001) 232.
[26] J.R. Barker, International Journal of Chemical Kinetics 41 (2009) 748.
[27] S.C. Smith, R.G. Gilbert, International Journal of Chemical Kinetics 20 (1988) 979.
[28] J.A. Miller, S.J. Klippenstein, The Journal of Physical Chemistry A 110 (2006) 10528.
[29] M. Akbar Ali, A. Violi, The Journal of Organic Chemistry 78 (2013) 5898.
[30] H. Hippler, J. Troe, H. Wendelken, The Journal of Chemical Physics 78 (1983) 6709.
[31] W. Forst, Unimolecular Reactions: A Concise Introduction, Cambridge University Press, 2003.
[32] R. Zellner, Berichte der Bunsengesellschaft für physikalische Chemie 81 (1977) 877.
[33] J.R. Barker, M. Frenklach, D.M. Golden, The Journal of Physical Chemistry A 119 (2015) 7451.